Ahmed, U, Malkeson, SP, Pillai, AL, Chakraborty, N and Kurose, R

 Flame self-interaction during turbulent boundary layer flashback of hydrogen-rich premixed combustion

https://researchonline.ljmu.ac.uk/id/eprint/19551/

Article

http://researchonline.ljmu.ac.uk/

Flame self-interaction during turbulent boundary layer flashback of hydrogen-rich premixed combustion

Umair Ahmed ●,[1,*] Sean P. Malkeson,[2] Abhishek L. Pillai ●,[3]
Nilanjan Chakraborty ●,[1] and Ryoichi Kurose ●[3]

[1]*School of Engineering, Newcastle University, Newcastle upon Tyne NE1 7RU, United Kingdom*
[2]*School of Engineering, Liverpool John Moores University, Liverpool L3 3AF, United Kingdom*
[3]*Department of Mechanical Engineering and Science, Kyoto University, Kyoto Daigaku-Katsura,
Nishikyo-ku, Kyoto 615-8540, Japan*

A three-dimensional direct numerical simulation database of turbulent boundary layer flashback of a hydrogen-rich premixed flame with an equivalence ratio of 1.5 has been analyzed to investigate flame self-interaction (FSI) events. The nonreacting turbulence characteristics of the channel flow are representative of the friction-velocity-based Reynolds number, $Re_\tau = 120$. A skeletal chemical mechanism with nine species and twenty reactions is employed for the representation of hydrogen-air combustion. Three definitions of the reaction progress variable, c, based on the mass fractions of H_2, O_2, and H_2O, have been considered to define the progress variable. It is found that the FSI events predominantly occur close to the burned gas side for all definitions of c at all the wall normal distances. No FSI events adjacent to the wall have been identified for the c definition based on O_2 and H_2O mass fractions, whereas FSI events occur for c based on H_2 in the near-wall region. In the regions further away from the wall, all c definitions show that tunnel formation and tunnel closure type FSI events remain predominant, which is consistent with the earlier findings by Griffiths *et al.* [Proc. Combust. Inst. **35**, 1341 (2015)] involving hydrogen-air premixed flame under shear flow conditions. In this work for c based on H_2 mass fraction, unburned gas pockets have also been identified at all wall normal distances and are a consequence of the hydrogen-rich nature of the flame. The reason for the variations in topologies with the change in the definition of c based on different species and wall normal distance is a consequence of several factors, including the changes in the level of turbulence within the turbulent boundary layer, heat loss to the isothermal wall in the near-wall region, and the differential diffusion induced by the nonunity Lewis number. The results from the current analysis show that the turbulent boundary layer and heat loss at the wall play important roles in determining the FSI topologies. The differences in the qualitative nature and distributions of the FSI events between different definitions of c have important implications on the possible extension of flame-surface-based modeling methodology for hydrogen-rich flames within turbulent boundary layers.

---

*umair.ahmed@newcastle.ac.uk

I. INTRODUCTION

High hydrogen content fuels are being considered as an alternative fuel for clean and efficient large-scale power generation [1]. This mode of combustion offers a lower environmental impact and higher energy efficiency [2]. Among the many challenges in enabling hydrogen-rich combustion for gas turbine applications, a fundamental understanding of flame flashback especially for unconventional and highly reactive hydrogen-rich fuels remains an open question [3]. Specifically, compared with hydrocarbon-air flames, hydrogen-air premixed flames are able to propagate three times (in relation to the flame thickness) closer to the wall before the heat loss to the solid surface leads to quenching [4].

The shape of turbulent premixed flames is a characteristic which needs to be understood for improving models for large eddy simulation (LES), especially in the case of models relying on the flame surface description, such as the G equation and flame surface density [5]. In these modeling frameworks, the flame shape or morphology characteristics are used for modeling premixed turbulent combustion [6,7]. In most practical combustion applications, turbulence-flame and flame-flame interactions (FFI) or flame self-interaction (FSI) are the dominant mechanism by which the flame shape is altered in time and space. The main difference between FFI and FSI events lies in the fact that the interaction of two different flames like twin V flames [8] is involved in the case of FFI, whereas in the case of FSI the flame elements from the same flame interact with each other due to wrinkling caused by turbulence [5,9], as shown in the sketches presented in Fig. 1. Typically the flame area tends to increase with turbulence, but the FFI-FSI events tend to decrease the flame surface area through the flame annihilation process [10,11]. The topological structures involved in turbulent boundary layer flashback are not well understood and need to be explored for a better physical understanding of the flame behavior. The concept of local flame structures based on the scalar fields, such as reaction progress variable, is important for the fundamental understanding of flame propagation statistics due to its role in flame surface generation and overall burning rate.

The relationship between geometrical structures and the gradient of scalar fields in turbulent flows has been considered in the pioneering work by Gibson [12]. According to Moffatt [13], the topological structures can be described by using the critical points as elliptic or hyperbolic according to the signature of the eigenvalues of the scalar Hessian tensor. The flame topologies play an important role in characterizing the FFI or FSI events in turbulent combustion processes [5,8,14–17]. Several approaches have been used in the literature for identifying FFI, including critical point theory [9,14,15], Minkowski functional [5,16], and automatic feature extraction technique based on complex wavelet transform [8]. In comparison to the existing body of literature on FFI involving freely propagating premixed flames [5,14,18], there is limited information available on this topic for wall-bounded premixed flames. In this spirit, the main objectives of the present work are to understand the flame self-interactions during boundary layer flashback of a hydrogen-rich premixed flame at different distances away from the wall. The aim is to investigate the influence of turbulence on the behavior of the FSI events, as well as the choice of the species used to identify FSI events.

The reset of the paper is organized as follows. In the next section, a brief mathematical background for the method used to identify FSI events is provided. This is followed by the description of the direct numerical simulation (DNS) data used for the analysis, which is followed by the results and the associated discussion. The conclusions are drawn and summarized in the final section.

II. MATHEMATICAL BACKGROUND

The reaction progress variable can be defined as

$$c \equiv \frac{Y_k - Y_k(\xi)_R}{Y_k(\xi)_P - Y_k(\xi)_R}, \tag{1}$$

where Y_k represents the mass fraction of species k, ξ represents the local mixture fraction, and the subscripts R and P indicate the respective values of the species in the unburned gases for the local
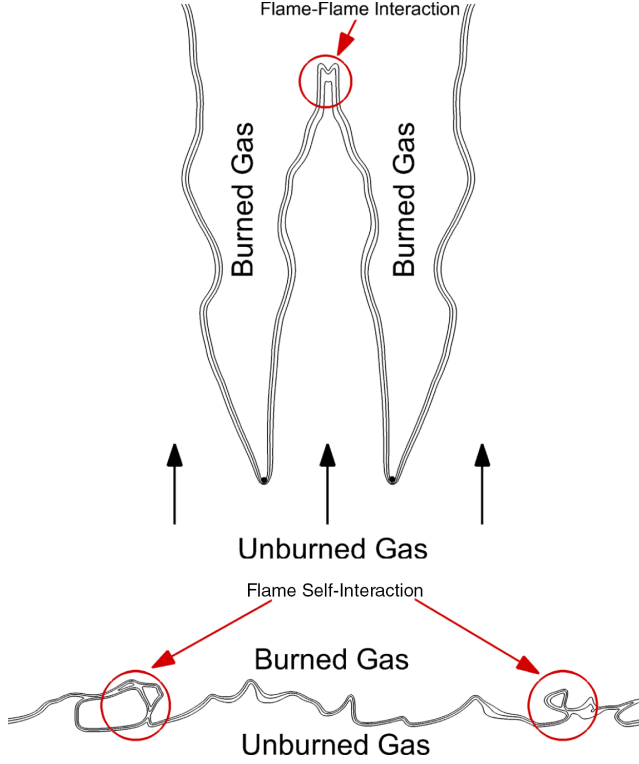
FIG. 1. Sketches of flame-flame interaction (FFI) in a twin V-flame (top) and flame self-interaction (FSI) in a flame encountering shear flow (bottom).

value of ξ and fully burned gases according to the equilibrium solution for the local value of ξ. The mixture fraction ξ is defined using Bilger's definition as [19]

$$\xi = \frac{\beta - \beta_O}{\beta_f - \beta_O}, \tag{2}$$

where $\beta = 2Y_C/W_C + 0.5Y_H/W_H - Y_O/W_O$, $\beta_f = (2a + 0.5b - c)/W_{C_aH_bO_c}$ (where $a = 0$, $b = 2$, and $c = 0$), and $\beta_O = -Y_{O\infty}/W_O$, with $Y_{O\infty}$ being the elemental oxygen mass fraction in the pure oxidizer stream; Y_M and W_M are the mass fraction and molecular mass of the element or species M, respectively. The equivalence ratio dependence of $Y_k(\xi)_R$ and $Y_k(\xi)_P$ are considered here because of possible modifications of equivalence ratio due to differential diffusion effects within the flame. The behavior of the critical points within the flame in relation to the reaction progress variable is of central importance for the identification of flame topologies [14,15]. Note that the gradient of c vanishes at the critical points within the flame, and consequently, the Taylor series expansion around a critical point can be written as follows [14]

$$c(\mathbf{a} + \mathbf{x}) = c(\mathbf{a}) + \frac{\mathbf{x}^T}{2}\underline{\underline{\mathbf{H}}}[c(\mathbf{a})]\mathbf{x} + \cdots, \tag{3}$$

such that the Hessian $\underline{\underline{\mathbf{H}}}(c)$ describes the local field to second-order accuracy. In this case the eigenvalues ($\lambda_1 > \lambda_2 > \lambda_3$) of $\underline{\underline{\mathbf{H}}}(c)$ are real, giving the curvature along each of the three orthogonal principal axes. If the orientation is considered to be unimportant, these eigenvalues fully define the local topology to second order [14]. The normalized shape factors θ and ϕ, which define a
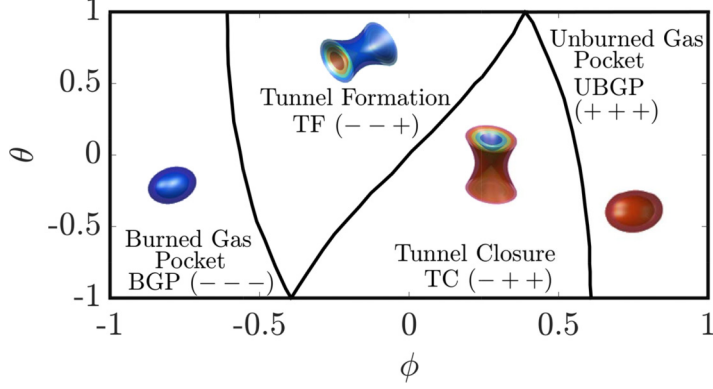
FIG. 2. Flame-flame interaction or flame self-interaction topologies characterized by the shape factors described in Eqs. (4) and (5). The sign of eigenvalues for $\underline{\underline{\mathbf{H}}}(c)$ is shown in each quadrant, with the black line indicating the change in the sign of eigenvalues. The shapes for the topologies are exemplarily shown (with the reaction progress variable value increasing from blue to red) and do not represent all of the possible topologies.

continuous two-dimensional domain fully describing the range of local topology of FSI events, can be defined based on the eigenvalues of $\underline{\underline{\mathbf{H}}}(c)$ and are expressed as [14]

$$\theta = \frac{6}{\pi}\arctan\left(\frac{(\lambda_1 - 2\lambda_2 + \lambda_3)/\sqrt{6}}{(\lambda_1 - \lambda_3)/\sqrt{2}}\right), \tag{4}$$

$$\phi = \frac{2}{\pi}\arctan\left(\frac{(\lambda_1 + \lambda_2 + \lambda_3)\cos\left(\frac{\theta\pi}{6}\right)/\sqrt{3}}{(\lambda_1 - \lambda_3)/\sqrt{2}}\right). \tag{5}$$

The FSI topologies in θ–ϕ space are shown in Fig. 2, where the sign of the eigenvalues of $\underline{\underline{\mathbf{H}}}(c)$ (from left to right in Fig. 2) changes from $(- - -)$ to $(- - +)$ to $(- + +)$ to $(+ + +)$. The black lines in Fig. 2 indicate the change in the sign of the eigenvalues. On the right-hand side of Fig. 2, the eigenvalues with the signs of $(+ + +)$ correspond to unburned gas pockets (UBGPs), whereas on the left-hand side of Fig. 2, the eigenvalues with the signs of $(- - -)$ represent burned gas pockets (BGPs). The intermediate combinations of eigenvalues between the left-hand side and right-hand side of Fig. 2 with signs of $(- - +)$ to $(- + +)$ represent tunnel formation (TF) and tunnel closure (TC) events, respectively. From a physical perspective, a TC topology is a cylindrical flame topology which propagates inward, whereas a TF topology grows outward in a cylindrical manner.

III. DIRECT NUMERICAL SIMULATION DATA

The DNS data of boundary layer flashback performed by Kitano *et al.* [20] has been considered for this analysis. The flow configuration, turbulence and flame characteristics are similar to the one used in the earlier work of Gruber *et al.* [4]. The DNS is representative of flashback in a channel flow at bulk Reynolds $Re_b = \rho u_b 2h/\mu = 3500$, where h is the channel half height, $u_b = 1/2h\int_0^{2h} u\,dy = 19.83$ m/s, and Reynolds number based on the channel half height and friction velocity $Re_\tau = \rho u_\tau h/\mu = 120$, with $u_\tau = \sqrt{|\tau_w|/\rho}$ and $\tau_w = \mu\partial u/\partial y|_{y=0}$ or $_{y=2h}$ being the friction velocity and wall shear stress, respectively. The simulation has been performed using the code known as FK^3, which has been used in several previous studies on turbulent, reacting, and multiphase flows [21,22]. The code solves conservation equations for mass, momentum, enthalpy, and chemical species in the context of finite-volume framework. A skeletal chemical mechanism

comprising nine chemical species and 20 reactions [23] is used to represent hydrogen-air combustion. The spatial derivatives for the momentum equation are evaluated via a fourth-order centered scheme. The convective terms of enthalpy and species mass fractions are calculated by using a third-order quadratic upstream interpolation for convective kinematics (QUICK) [24] scheme. A second-order centered scheme is used to calculate all the other terms in the scalar transport equations. The pressure-based semi-implicit algorithm for compressible flows proposed by Moureau *et al.* [25] is used to solve the equations. The multicomponent diffusion for different chemical species is evaluated via the diffusion velocities by solving the system of linear equations proposed in Refs. [26,27] for all grid points, at all time steps and in all directions. The binary diffusion coefficients required for diffusion calculation are obtained from CHEMKIN [28]. Further details on the numerical techniques used in this simulation can be found in the earlier work of Kitano *et al.* [20].

The channel flow in this simulation is subdivided into two parts, the turbulence generation region and the flashback region, as shown in Refs. [20,29]. The dimensions of the channel flow region are 173 mm×20 mm×30 mm, of which the flashback region consists of 103 mm×20 mm×30 mm. In the turbulence generation region of the channel flow, a fully developed wall-bounded turbulent flow is generated by imposing a pressure drop and a periodic boundary condition in the x direction. Further details on the nonreacting turbulence introduced into the flashback region of the channel can be found in Ref. [29]. In the flashback region of the channel, the outflow characteristics of the upstream channel are introduced and a freely propagating planar flame is initialized in the domain after 100 ms of the flow becoming fully turbulent in the channel. A no-slip isothermal boundary condition at 750 K is applied on the walls in the y direction, while the z direction is treated as periodic. The Navier-Stokes characteristic boundary condition (NSCBC) [30] is applied at the outflow boundaries. The initial gas temperature, pressure, and equivalence ratio are 750 K, 0.1 MPa, and 1.5, respectively. The laminar burning velocity S_L and the thermal flame thickness $\delta_{\mathrm{th}} = (T_{\mathrm{ad}} - T_R)/\max|\nabla T|_L$ (where T_R is the reactant temperature, T_{ad} is the adiabatic flame temperature and the subscript L represents the laminar flame quantities) under these conditions are determined to be 14 m/s and 0.48 mm, respectively [31]. The grid resolution in the flashback region of the simulation is 50 μm, which in nondimensional wall units is $\Delta x^+ = \Delta y^+ = \Delta z^+ = 0.6$. This level of resolution is appropriate, as it ensures that the laminar flame thermal thickness δ_{th} is resolved in approximately ten grid points and satisfies the resolution criteria for turbulent boundary layers, as recommended by Moser *et al.* [32]. Larger grid spacing of 700 μm ($\Delta x^+ = 8.4$) is used in the x direction of the turbulence generation region of the simulation, as this level of resolution is sufficient to resolve the nonreacting turbulence at the conditions used in this work. A total of approximately 0.4 billion grid points are used in the simulation, of which 1150×400×600 are in the flashback region of the simulation. Note that in the current DNS the integral length scale based on the two-point correlation remains large and the turbulence intensity remains low towards the center of the channel, as is the case in turbulent channel flows [33–35]. The variation of the longitudinal integral length scale remains of the order of channel half height at low Re_τ, which is consistent with previous studies [35]. The channel half height in this case is 0.01 m and the thermal flame thickness is 0.48 mm, while the maximum root-mean-square velocity is of the order of 2 m/s, which is lower in comparison to the laminar flame speed of 14 m/s. This implies that the conditions investigated in this work have some attributes (e.g., the turbulent integral length scale) of the actual gas turbine operating conditions. It should be noted here that in most gas turbine applications, combustion occurs at higher than atmospheric pressure conditions. Under these conditions the fluid dynamics is not significantly affected, whereas the thermodynamics and chemical processes are affected such that the laminar burning velocity and the thermal flame thickness decrease. This results in the conditions where the thermal flame thickness is much smaller than the integral length scale [36], which in turn triggers the hydrodynamic instability commonly known as Darrieus-Landau instability [4,36]. This implies that the conditions investigated in this work have some attributes of the actual gas turbine operating conditions. It is worth noting the vast majority of analyses on computational simulations and modeling of turbulent premixed flames have been carried out for atmospheric
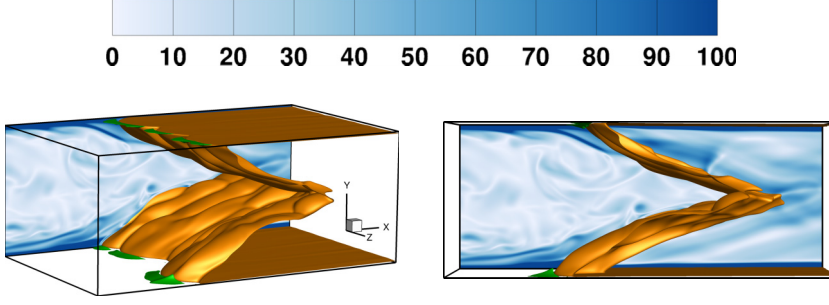
FIG. 3. Instantaneous distributions of isosurfaces of the temperature at 1700 K (colored in yellow) and the instantaneous normalized vorticity magnitude in the flashback region of the channel. The negative flow velocity regions are shown on the top and bottom walls (green color).

pressure for the purpose of computational economy, and the same approach was adopted in previous analyses on boundary layer flashback [4,37,38] and FFI/FSI topologies [14,15,18].

In the current analysis, the data is sampled after 1.6 ms from the time when the flame is initialized in the domain, which ensures that a steady flashback speed has been attained, and a further explanation of this is provided in the earlier work of Kitano *et al.* [20]. Three definitions for reaction progress variables based on H_2, O_2, and H_2O mass fractions have been used to identify the FSI events. In this work the flashback region of the computational domain is considered and the statistics are conditioned on c across the range of $0.01 \leqslant c \leqslant 0.99$, which ensures that the identification of the FSI topologies is limited to those locations where combustion occurs. The results shown in the next section of the paper involve relevant quantities conditioned upon a particular c value for a given value of y/h. A similar procedure was followed in several previous studies on the analysis of FFI/FSI [14,15,18].

IV. RESULTS AND DISCUSSION

Figure 3 shows the instantaneous isosurface of temperature at 1700 K and the vorticity magnitude field within the flashback region of the flow. It can be seen from Fig. 3 that the flame alters the boundary layer structure and the temperature isosurface is wrinkled by the oncoming turbulence. Furthermore, Fig. 3 demonstrates that the turbulence decays across the flame in the near-wall region, whereas turbulence is generated in the middle of the channel due to the merging of the two flame branches from the top and bottom walls [29]. Figure 3 also shows the localized reverse flow regions of the flow (green isosurfaces), which are clearly visible immediately upstream of each flame bulge and are limited to the near-wall region. This behavior is consistent with the earlier findings of Gruber *et al.* [4]. The physical mechanism which leads to these reverse flow regions upstream of the flame has been discussed elsewhere [4,29] and thus is not repeated here. Figure 3 also demonstrates that in the case of turbulent boundary layer flashback the flame topology changes with the distance away from the wall. It has been shown earlier [39] that the behaviors of the surface density function (SDF), represented by $|\nabla c|$, and the flame displacement speed, $S_d = |\nabla c|^{-1}(Dc/Dt)$, are significantly affected by the choice of the species mass fraction used to define the progress variable as well as the distance away from the wall. Thus all the following results in this work are presented at $y/h = 0.005$, $y/h = 0.5$, and $y/h = 1.0$ locations, which are representative of nondimensional wall distance in the nonreacting channel, $y^+ = (\rho u_\tau y)/\mu$, of 0.6,60 and 120.

The behavior of the shape factors at different distances away from the wall based on different definitions of c are shown in Fig. 4. It is evident from Fig. 4 that in the case of c based on Y_{H_2}, all four FSI topologies occur within the flame across all wall normal distances, whereas in the case of c based on Y_{O_2} and Y_{H_2O}, no FSI events occur in the vicinity of the wall and the FSI events start to occur as the distance from the wall increases. It should be recognized here that in
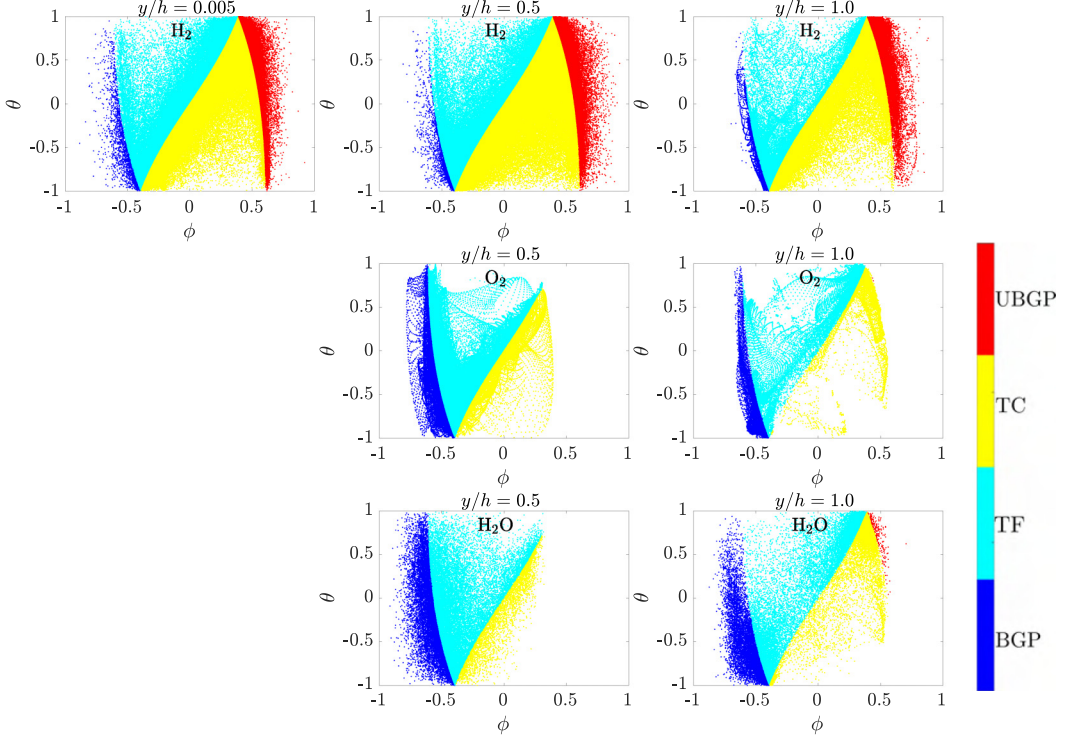
FIG. 4. Scatter plots of θ vs ϕ for $0.01 \leqslant c \leqslant 0.99$ at $y/h = 0.005$, $y/h = 0.5$, and $y/h = 1.0$ for c based on Y_{H_2}, Y_{O_2}, and Y_{H_2O}. Note that no critical points exist for c based on Y_{O_2} and Y_{H_2O} at $y/h = 0.005$.

the near-wall region (i.e., $y/h = 0.005$) no critical points exist in the case of c based on O_2 and H_2O mass fractions, as the reaction rate for H_2 is negligible in this region and a small displacement speed has been reported for H_2 in this region in the earlier work [39]. The faster displacement speed of c isosurfaces for Y_{O_2} and Y_{H_2O} based c than in the case of Y_{H_2} based c suggests that the FSI events remain rare for Y_{O_2} and Y_{H_2O} based c because they cannot exist for long. The presence of all four topologies and especially unburned gas pockets is expected in the case of c based on Y_{H_2}, as unburned gas pockets exist at all the sampling locations due to the hydrogen-rich nature of the flame. In the case of c based on Y_{O_2} and Y_{H_2O} at $y/h = 0.5$, only the topologies associated with burned gas pockets, tunnel formation, and tunnel closure can be seen in Fig. 4, and further away from the wall at $y/h = 1.0$ almost all four topologies exist (see Fig. 4). The Lewis number of H_2 is 0.3, whereas the Lewis numbers of O_2 and H_2O are 1.1 and 0.83, respectively, which suggests that the preferential diffusion effects due to nonunity Lewis number can potentially play a key role in determining the Y_{H_2} based c isosurface topologies, whereas the preferential diffusion effects are relatively weaker for Y_{O_2} and Y_{H_2O} based c in comparison to Y_{H_2} based c. The differences in reaction rate for different definitions of c in addition to the preferential diffusion also play a significant role in determining the c isosurface topology distributions. In the case of c based on Y_{O_2} and Y_{H_2O} at $y/h = 0.5$ and $y/h = 1.0$, the interaction events are strongly clustered along the lines within the space where the eigenvalues change sign. This type of clustering corresponds to interactions which are predominantly two-dimensional, such as two ridges meeting or expansion and/or contraction of a cylindrical tunnel of products or reactants [14].

Figure 5 shows the frequency of the FSI topologies for different values of c for all the definitions used. In the near-wall region at $y/h = 0.005$, only the c definition based on Y_{H_2} has FSI events and has the highest frequencies when compared with other distances away from the wall at $y/h = 0.5$
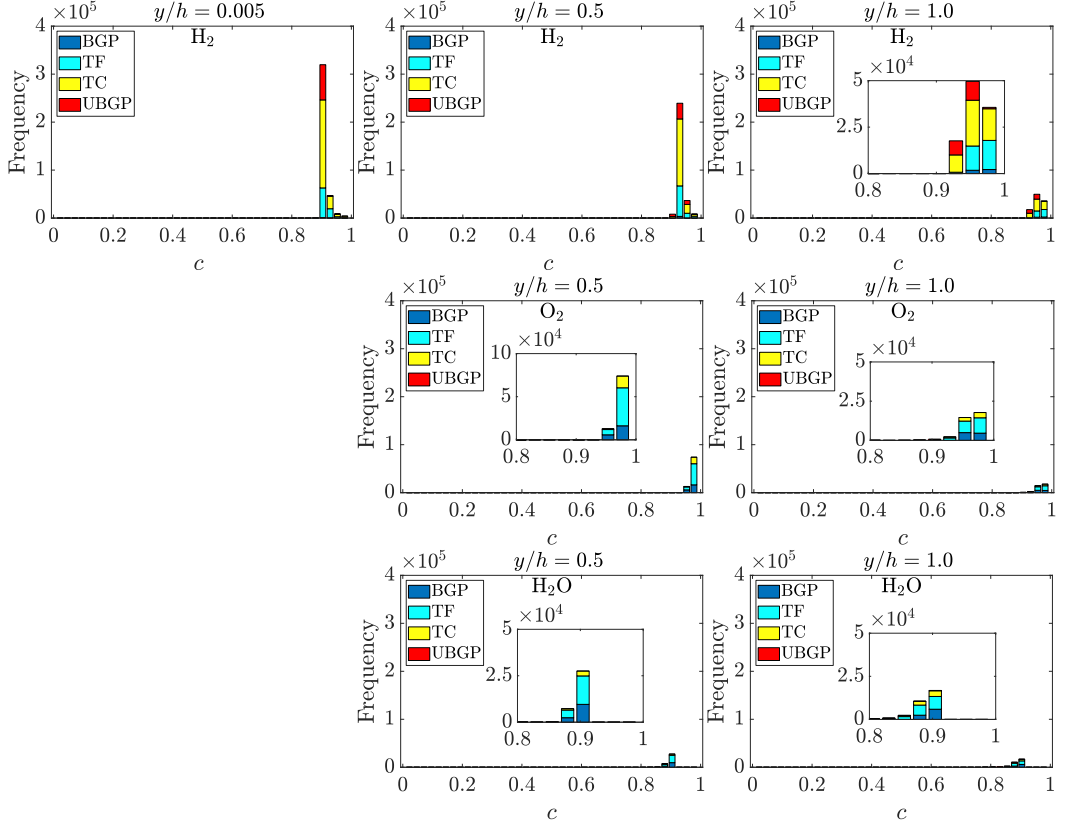
FIG. 5. Histograms of the number of samples of FSI topologies for $0.01 \leqslant c \leqslant 0.99$ at $y/h = 0.005$, $y/h = 0.5$, and $y/h = 1.0$ for c based on Y_{H_2}, Y_{O_2}, and Y_{H_2O}. Note that no critical points exist for c based on Y_{O_2} and Y_{H_2O} at $y/h = 0.005$.

and $y/h = 1.0$. In the case of c based on Y_{O_2} and Y_{H_2O}, higher frequencies for FSI events are observed at $y/h = 0.5$ when compared with the FSI frequencies at the center of the channel at $y/h = 1.0$. The topologies associated with the FSI events are predominantly found near the burned gas region corresponding to $0.8 \leqslant c \leqslant 0.99$ for all the sampling locations and definitions of c. The main reason for this behavior is due to the fact that the Re_τ of the channel is low, leading to a low turbulence intensity and a large longitudinal integral length scale [35]. This combination in turn wrinkles the flame structure, but turbulence cannot enter the flame structure and perturbs the leading edge of the flame to a level which would result in FSI events. Moreover, due to the large integral length scale the ratio of integral length scale to flame thickness can be above the threshold for which hydrodynamic instability, such as Darrius-Landau instability, can develop. Although this instability and background turbulence affect each other in a complex manner, their individual influence is not straightforward to isolate for a coupled system—like in the current simulation where large-scale flame wrinkles are induced by the combined actions of turbulence and Darrieus-Landau instability. More specific simulations and experiments can be performed to isolate these effects, which is beyond the scope of current work.

The large-scale wrinkles caused by turbulence and hydrodynamic instability in this case lead to FSI events at the trailing edge of the flame. The existence of FSI events at the trailing edge of lean hydrogen flames under high Damköhler number conditions in a shear layer has been reported by Griffiths *et al.* [14] in the case of c based on Y_{H_2O} and by Trivedi *et al.* [15] in the case of c based
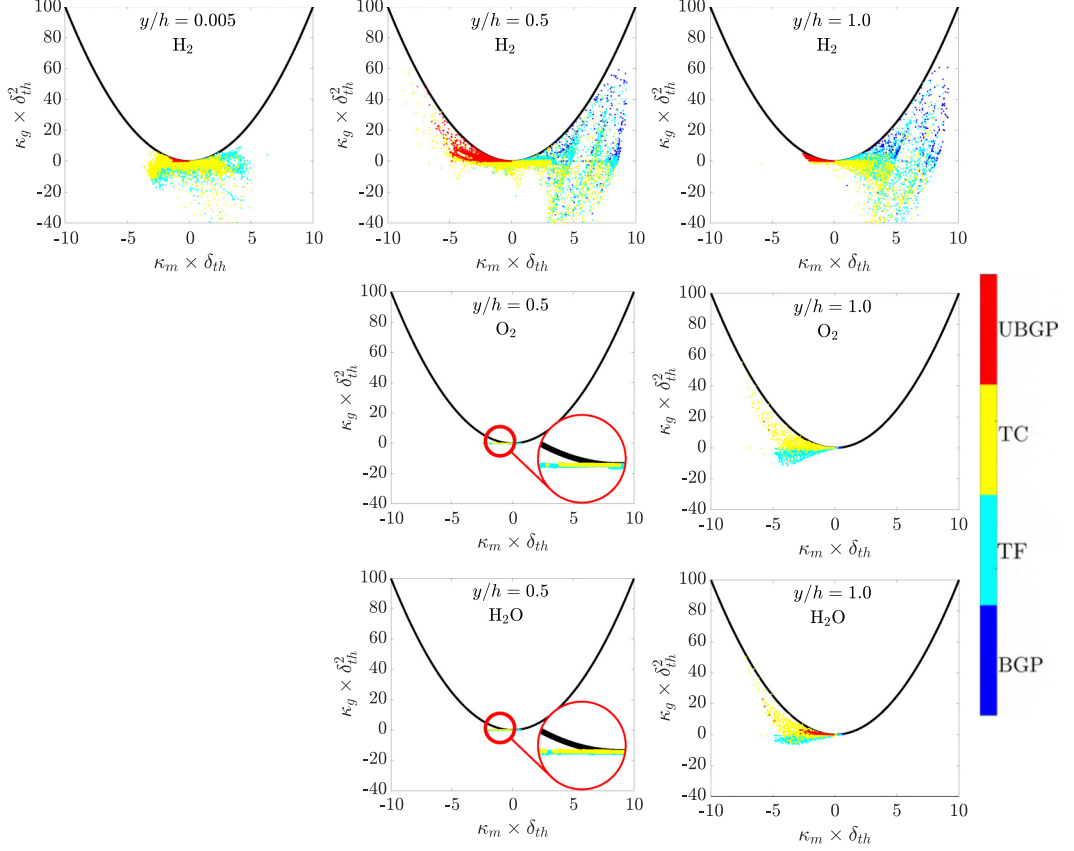
FIG. 6. Scatter of $\kappa_g \times \delta_{th}^2$ vs $\kappa_m \times \delta_{th}$ at the critical points for $0.01 \leqslant c \leqslant 0.99$ at $y/h = 0.005$, $y/h = 0.5$, and $y/h = 1.0$ for c based on Y_{H_2}, Y_{O_2}, and Y_{H_2O}. Note that no critical points exist for c based on Y_{O_2} and Y_{H_2O} at $y/h = 0.005$.

on Y_{H_2}. Figure 5 shows that the "pocket" events are relatively rare by comparison with the other two types of behavior (i.e., tunnel formation and tunnel closure). In the case of c based on Y_{H_2}, higher frequencies of unburned gas pockets are observed at all y/h locations when compared with the corresponding frequencies for Y_{O_2} and Y_{H_2O} based c, which is due to the hydrogen-rich nature of the flame. Overall, the low occurrence of unburned gas pockets at all sampling locations is due to the transient nature of such an event, as unburned gas pockets are surrounded by hot products and the reactants are rapidly consumed [11]. This behavior is consistent with the earlier works [14,15] involving lean hydrogen flames in shear layers.

The local flame surface geometries can be further categorized based on the local mean curvature, $\kappa_m = 0.5\nabla \cdot (-\nabla c/|\nabla c|) = (\kappa_1 + \kappa_2)/2$, and Gauss curvature $\kappa_g = \kappa_1\kappa_2$ [40], where κ_1 and κ_2 are the two principal curvatures. According to these definitions, the region given by $\kappa_g > \kappa_m^2$ is unrealizable because it leads to complex principal curvatures, while positive values of κ_g imply elliptic cuplike topologies, and negative values of κ_g values represent hyperbolic saddle geometries [40]. A negative (positive) value of κ_m indicates the flame surface in question remains concave (convex) to the reactants [40]. The locations at which κ_g vanishes exhibit tile convex (concave) geometries for $\kappa_m > 0$ ($\kappa_m < 0$) or flat topologies for $\kappa_m = 0$ [40]. Figure 6 shows the scatters of the different FSI events in the region corresponding to $0.01 \leqslant c \leqslant 0.99$ in the κ_m–κ_g plane for all the definitions of c and all sampling locations away from the wall. In the case of c based on Y_{H_2},

the unburned gas pockets (i.e. geometries propagating inwards) predominantly exhibit concave tile topologies, although concave cuplike geometries are also possible at $y/h = 0.5$, but this tendency decreases with increasing wall normal distance. Tunnel formation and tunnel closure events can also be seen for c based on Y_{H_2} in Fig. 6, where it can be seen that the tunnel formation and tunnel closure events are associated with hyperbolic saddle geometries and according to Fig. 5 show the highest frequencies. Further away from the wall (i.e., $y/h = 0.5$ and $y/h = 1.0$) for c based on Y_{H_2}, burned gas pockets (i.e., geometries propagating outwards) can also be found and are associated with convex cuplike topologies (see Fig. 6). As mentioned before, there are no critical points in the near-wall region (i.e., $y/h = 0.005$) for c based on Y_{O_2} and Y_{H_2O}, and hence no FSI events are recorded. Further away from the wall at $y/h = 0.5$ and $y/h = 1.0$ in the case of c based on Y_{O_2} and Y_{H_2O}, tunnel formation and tunnel closure events can be seen in Fig. 6. In this case c based on both Y_{O_2} and Y_{H_2O} behaves in a similar manner, and tunnel formation and tunnel closure events are predominantly associated with concave tile-type topologies, although towards the center of the channel at $y/h = 1.0$ some concave cuplike and concave saddlelike topologies are also possible, as shown in Fig. 6. It should be noted here that in the case of c based on both Y_{O_2} and Y_{H_2O}, a negligibly small amount of unburned gas pockets are identified at $y/h = 1.0$, as shown in Fig. 5, and are associated with tile concave topologies. Overall, the behavior of the topologies changes from the near-wall region (i.e., $y/h = 0.005$) to the center of the channel (i.e., $y/h = 1.0$) due to the variation of turbulence encountered by the flame at different wall normal distances—as turbulence fluctuations vary significantly with wall normal distance in fully developed boundary layers—as well as the fact the two flame branches from the top and bottom walls merge at the channel centerline. It should be recognized here that the turbulence fluctuations vary for all (streamwise, wall normal and transverse) components of velocity in the wall normal direction, while the dominant fluctuation (two to three times in magnitude) is for the streamwise component of velocity, and this has been shown in several works [32,34,41] on turbulent channel flows for a range of Re_τ values. So, crosswise or spanwise spatial fluctuations of velocity will not have a significant influence on the flame statistics reported in this analysis. This is also consistent with the earlier work of Griffiths *et al.* [14] and Trivedi *et al.* [15] in the case of shear layer flows where the streamwise velocity fluctuations are dominant when compared with the crosswise or spanwise spatial fluctuations of velocity. Further details on the behavior of turbulent kinetic energy and its dissipation, along with the behavior of wall shear stresses, Reynolds stresses, and the individual terms in the turbulent kinetic energy transport equation are presented in Ref. [29] for this DNS database and are not repeated here for the sake of brevity.

The aforementioned variation in topologies can be further investigated by interrogating c isosurfaces based on Y_{H_2}, Y_{O_2}, and Y_{H_2O}. The variation in the topology of c based on different definitions can be noticed in Fig. 7, and it can also be seen that c based on Y_{H_2} mass fraction has streaks of unburned fuel on the walls. This is consistent with the findings in Fig. 5, where a significant frequency of the unburned gas pockets have been recorded at almost all y/h locations, but the frequency decreases with increasing wall normal distance. Furthermore, Fig. 7 shows that the c based on Y_{H_2} experiences the highest magnitude in the values of κ_m throughout the domain which arises due to greater extent of flame wrinkling induced by stronger preferential diffusion as a result of small Lewis number of H_2. Figure 7 also shows that all the c definitions tend to form local tunnel-like shapes due to the flame wrinkling, and this trend is prevalent at all wall normal distances away from the wall. This trend is consistent with the identification of tunnel formation and tunnel closure events, identified as the highest frequency events in Fig. 5.

For the purpose of completeness, it is worth noting that the equivalence ratio varies at most by 10% across the flame in the case considered here. Furthermore, in this case when using the standard definition for progress variable [when $(Y_k)_R$ and $(Y_k)_P$ are not taken to be local functions of ξ], the values for progress variable do not change appreciably in comparison to the prediction of Eq. (1) for the respective species used, and the same frequency of occurrence of different topologies for different species is obtained as the one obtained from the progress variable definition relying on local equivalence ratio variations. It should also be noted here that the standard definition of
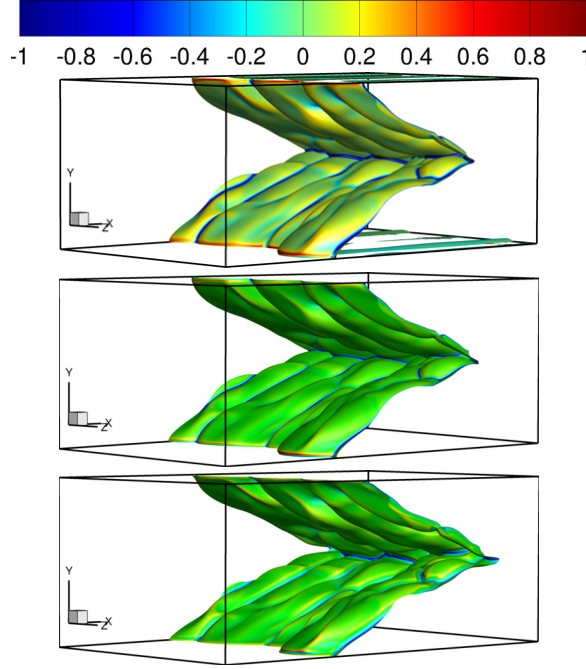
FIG. 7. Instantaneous isosurface of $c = 0.9$ colored by $\kappa_m \times \delta_{th}$ for c based on Y_{H_2} (top), Y_{O_2} (middle), and Y_{H_2O} (bottom).

the progress variable without any local mixture fraction dependence has been extensively used for turbulent premixed hydrogen flames [14,15,42]. In previous works on premixed hydrogen-air premixed flames, the progress variable has been defined based on O_2 [42], H_2O [14], and H_2 [15] mass fractions. Furthermore, flame-topology-based analysis has been performed in Refs. [14,15] based on the standard premixed definition of the progress variable involving H_2O and H_2 mass fractions, respectively.

The differences in the topology distributions for FSI events between different species and wall normal distances indicate that the flame surface area annihilation because of FSI is expected to be different across the turbulent boundary layer encountered in channel flows. From a modeling perspective, further insights into the flame-flame interaction can be achieved by considering the statistical behaviors of the displacement speed S_d of the reaction progress variable and the surface density function $|\nabla c|$. The transport equation for the reaction progress variable c can be written as

$$\rho \frac{\partial c}{\partial t} + \rho u_j \frac{\partial c}{\partial x_j} = \frac{\partial}{\partial}\left(\rho D \frac{\partial c}{\partial x_j}\right) + \dot{\omega}_c + A_c, \tag{6}$$

where ρ is the density, u_j is the jth component of velocity, D is the diffusivity of the progress variable, and $\dot{\omega}_c$ is the reaction rate of c and A_c arises due to the local mixture fraction variations. The transport equation of c can be written in kinematic form for a given c isosurface as

$$\left(\frac{\partial c}{\partial t} + u_j \frac{\partial c}{\partial x_j}\right) = S_d |\nabla c|, \tag{7}$$

where S_d is defined as [43,44]

$$S_d = \frac{\dot{\omega}_c + \nabla \cdot (\rho D \nabla c) + A_c}{\rho |\nabla c|}. \tag{8}$$

Now the transport equation for $|\nabla c|$ can be written as [45–47]

$$\frac{\partial |\nabla c|}{\partial t} + \frac{\partial (u_j |\nabla c|)}{\partial x_j} = a_T |\nabla c| - \frac{\partial (S_d N_j |\nabla c|)}{\partial x_j} + 2 S_d \kappa_m |\nabla c|, \tag{9}$$

where $a_T = (\delta_{ij} - N_i N_j)(\partial u_i / \partial x_j)$ is the tangential strain rate. The four principal flame topologies (i.e., UBGP, TF, TC, and BGP) can be represented based on the scaled local coordinates x, y, and z for small deviations from a critical point as follows [18]:

$$c(x, y, z) = c_0 + \tfrac{1}{2}x^2 + \tfrac{1}{2}y^2 + \tfrac{1}{2}z^2 \quad \text{for UBGP}, \tag{10}$$

$$c(x, y, z) = c_0 + \tfrac{1}{2}x^2 - \tfrac{1}{2}y^2 - \tfrac{1}{2}z^2 \quad \text{for TF}, \tag{11}$$

$$c(x, y, z) = c_0 - \tfrac{1}{2}x^2 + \tfrac{1}{2}y^2 + \tfrac{1}{2}z^2 \quad \text{for TC}, \tag{12}$$

$$c(x, y, z) = c_0 - \tfrac{1}{2}x^2 - \tfrac{1}{2}y^2 - \tfrac{1}{2}z^2 \quad \text{for BGP}, \tag{13}$$

where c_0 is the is the reaction progress variable value at the critical point. Based upon the expressions given by the above equations, it can be stated that an unburned gas pocket will correspond to a local minimum (i.e., a central low value of the reaction progress variable with surrounding higher values), whereas a burned gas pocket will correspond to a local maximum (i.e., a central high value of the reaction progress variable with surrounding lower values). For the UBGP topology, the normal vector N can be expressed as $N = (-x/r, -y/r, -z/r)^T$, where the radius $r = (x^2 + y^2 + z^2)^{1/2}$, and twice the curvature of the flame surface 2κ can be expressed as $2\kappa = -2/r$. In the case of BGP topology $N = (x/r, y/r, z/r)^T$ and $2\kappa = 2/r$. A tunnel formation topology corresponds to a local saddle point with a minimum on the central axis of the tunnel (taken as the x direction) with a maximum in the two other directions where a tunnel formation topology corresponds to a local saddle point with a maximum on the central axis of the tunnel (taken as the x direction) with a minimum in the two other directions. Accordingly, for the TF topology, $N = (-x/r, y/r, z/r)^T$ and $2\kappa = -2x^2/r^3$. For the tunnel closure topology, $N = (x/r, -y/r, -z/r)^T$ and $2\kappa = -2x^2/r^3$. Similarly, it is possible to evaluate the terms in the SDF transport equation using the expressions for N and 2κ in the case of FSI events, which is beyond the scope of the current analysis.

The behavior of the displacement speed S_d (including its components) and the evolution of the surface density function have been investigated in detail in [39] for this flame configuration. It has been demonstrated in [39] that the flame surface area is significantly affected by the variation of turbulence in the wall normal direction as well as the heat loss to the cold wall from the flame. The definition of c also plays a role in determining the overall flame behavior. The qualitative behavior in flame topology distributions for the FSI events found in this work implies that existing closure methodologies, including the flame surface density (FSD) approach [48,49], which depends on the flame surface topology, may need significant modifications to be valid for turbulent boundary layer flashback of hydrogen-air premixed flames.

V. CONCLUSIONS

The behaviors of flame self-interaction (FSI) events during flashback of a hydrogen-rich premixed flame in a turbulent channel flow have been investigated by interrogating a DNS database. The nonreacting turbulence characteristics of the channel flow are representative of the friction-velocity-based Reynolds number $Re_\tau = 120$, while a hydrogen-air mixture with an equivalence ratio of 1.5 has been considered. A detailed chemical mechanism with nine species and twenty reactions is employed for an accurate representation of hydrogen-air combustion. Different definitions based on mass fractions of H_2, O_2, and H_2O have been used to define the progress variable c. The FSI events have predominantly been found close to the burned gas side for all definitions of c at all the wall normal distances. No critical points adjacent to the wall have been found for the c definition based on Y_{O_2} and Y_{H_2O}, whereas FSI events occur for c based on H_2 in the near-wall region. Further away from the wall, all c definitions show FSI events, and the predominant topologies identified

represent tunnel formation and tunnel closure events, which is consistent with the earlier findings of Griffiths *et al.* [14]. In the current work for c based on Y_{H_2}, unburned gas pockets have also been identified and are a consequence of the hydrogen-rich nature of the flame. Overall, these variations in the existence of topologies with the change in the definition of c based on different species and wall normal distance are a consequence of several factors, including the variation of Lewis number among different species, differences in chemical reactions, changes in the level of turbulence within the turbulent boundary layer, heat loss to the isothermal wall, and also the fact that the flame considered in this work is hydrogen rich and leads to unburned H_2 within the domain. The results from the current analysis reported in this paper show that the turbulent boundary layer and the heat loss at the wall play important roles in determining the FSI topologies. The differences in the qualitative nature and distributions of the FSI events between different definitions of c have important implications on the possible extension of flame-surface-based modeling methodology for hydrogen-rich flames within turbulent boundary layers. Further work involving different air-fuel mixture equivalence ratios and turbulence conditions is needed for a more comprehensive understanding of FSI trends.

---

[1] O. Bolland and H. Undrum, A novel methodology for comparing CO_2 capture options for natural gas-fired combined cycle plants, Adv. Environ. Res. **7**, 901 (2003).

[2] T. C. Lieuwen, V. McDonell, E. Petersen, and D. Santavicca, Fuel flexibility influences on premixed combustor blowout, flashback, autoignition, and stability, J. Eng. Gas Turbines Power **130**, 011506 (2008).

[3] M. Ni, D. Y. Leung, M. K. Leung, and K. Sumathy, An overview of hydrogen production from biomass, Fuel Process. Technol. **87**, 461 (2006).

[4] A. Gruber, J. H. Chen, D. Valiev, and C. K. Law, Direct numerical simulation of premixed flame boundary layer flashback in turbulent channel flow, J. Fluid Mech. **709**, 516 (2012).

[5] Y. Minamoto, B. Yenerdag, and M. Tanahashi, Morphology and structure of hydrogen–air turbulent premixed flames, Combust. Flame **192**, 369 (2018).

[6] F. Gouldin, An application of fractals to modeling premixed turbulent flames, Combust. Flame **68**, 249 (1987).

[7] A. N. Lipatnikov and J. Chomiak, Molecular transport effects on turbulent flame propagation and structure, Prog. Energy Combust. Sci. **31**, 1 (2005).

[8] T. D. Dunstan, N. Swaminathan, K. N. C. Bray, and N. G. Kingsbury, Flame interactions in turbulent premixed twin V-flames, Combust. Sci. Technol. **185**, 134 (2013).

[9] G. Ozel-Erol, U. Ahmed, and N. Chakraborty, Flame self-interactions in globally stoichiometric spherically expanding flames propagating into fuel droplet-mists, Proc. Combust. Inst. **38**, 3351 (2021).

[10] T. Echekki, J. H. Chen, and I. Gran, The mechanism of mutual annihilation of stoichiometric premixed methane-air flames, Symp. Combust. **26**, 855 (1996).

[11] W. Kollmann and J. H. Chen, Pocket formation and the flame surface density equation, Symp. Combust. **27**, 927 (1998).

[12] C. H. Gibson, Fine structure of scalar fields mixed by turbulence, I. Zero-gradient points and minimal gradient surfaces, Phys. Fluids **11**, 2305 (1968).

[13] H. Moffatt, The topology of scalar fields in 2D and 3D turbulence, in *IUTAM Symposium on Geometry and Statistics of Turbulence, Fluid Mechanics and Its Applications*, edited by N. T. M. T. Kambe (Springer, New York, 2001), Vol. 59.

[14] R. A. Griffiths, J. H. Chen, H. Kolla, R. S. Cant, and W. Kollmann, Three-dimensional topology of turbulent premixed flame interaction, Proc. Combust. Inst. **35**, 1341 (2015).

[15] S. Trivedi, H. Kolla, J. H. Chen, and R. S. Cant, Analysis of flame-flame interactions in premixed hydrocarbon and hydrogen flames, Phys. Rev. Fluids **5**, 113201 (2020).

[16] N. A. K. Doan, N. Swaminathan, and Y. Minamoto, DNS of MILD combustion with mixture fraction variations, Combust. Flame **189**, 173 (2018).

[17] A. Tyagi, I. Boxx, S. Peluso, and J. O'Connor, The role of flow interaction in flame-flame interaction events in a dual burner experiment, Proc. Combust. Inst. **37**, 2485 (2019).

[18] S. Trivedi, R. Griffiths, H. Kolla, J. H. Chen, and R. S. Cant, Topology of pocket formation in turbulent premixed flames, Proc. Combust. Inst. **37**, 2619 (2019).

[19] R. Bilger, Turbulent flows with nonpremixed reactants, in *Turbulent Reacting Flows*, edited by P. Libby and F. Williams, Topics in Applied Physics Vol. 44 (Springer, New York, 1980), pp. 65–113.

[20] T. Kitano, T. Tsuji, R. Kurose, and S. Komori, Effect of pressure oscillations on flashback characteristics in a turbulent channel flow, Energy Fuels **29**, 6815 (2015).

[21] A. L. Pillai and R. Kurose, Combustion noise analysis of a turbulent spray flame using a hybrid DNS/APE-RF approach, Combust. Flame **200**, 168 (2019).

[22] A. L. Pillai, R. Kai, T. Murata, T. Ikedo, R. Masuda, and R. Kurose, Numerical analysis of heat transfer characteristics of spray flames impinging on a wall under CI engine-like conditions, Combust. Flame **239**, 111615 (2021).

[23] J. A. Miller and C. T. Bowman, Mechanism and modeling of nitrogen chemistry in combustion, Prog. Energy Combust. Sci. **15**, 287 (1989).

[24] B. Leonard, A stable and accurate convective modelling procedure based on quadratic upstream interpolation, Comput. Methods Appl. Mech. Eng. **19**, 59 (1979).

[25] V. Moureau, C. Bérat, and H. Pitsch, An efficient semi-implicit compressible solver for large-eddy simulations, J. Comput. Phys. **226**, 1256 (2007).

[26] F. A. Williams, *Combustion Theory*, 2nd ed. (CRC Press, Boca Raton, FL, 1994).

[27] A. Ern and V. Giovangigli, *Multicomponent Transport Algorithms* (Springer-Verlag, Heidelberg, 1994).

[28] R. Kee, F. Rupley, and J. A. Miller, *Chemkin-II: A FORTRAN Chemical Kinetics Package for the Analysis of Gas-Phase Chemical Kinetics*, Technical report, Sandia National Laboratories, Albuquerque, NM, Livermore, CA, 1989.

[29] U. Ahmed, A. L. Pillai, N. Chakraborty, and R. Kurose, Statistical behavior of turbulent kinetic energy transport in boundary layer flashback of hydrogen-rich premixed combustion, Phys. Rev. Fluids **4**, 103201 (2019).

[30] T. J. Poinsot and S. Lele, Boundary conditions for direct simulations of compressible viscous flows, J. Comput. Phys. **101**, 104 (1992).

[31] H. Pitsch, A C ++ Computer Program for 0D Combustion and 1D Laminar Flame Calculations, https://www.itv.rwth-aachen.de/downloads/flamemaster/

[32] R. D. Moser, J. Kim, and N. N. Mansour, Direct numerical simulation of turbulent channel flow up to $Re\tau = 590$, Phys. Fluids **11**, 943 (1999).

[33] H. Abe, H. Kawamura, and Y. Matsuo, Surface heat-flux fluctuations in a turbulent channel flow up to $Re\tau = 1020$ with Pr = 0.025 and 0.71, Int. J. Heat Fluid Flow **25**, 404 (2004).

[34] J. Kim, P. Moin, and R. D. Moser, Turbulence statistics in fully developed channel flow at low Reynolds number, J. Fluid Mech. **177**, 133 (1987).

[35] U. Ahmed, D. D. Apsley, T. Stallard, P. K. Stansby, and I. Afgan, Turbulent length scales and budgets of Reynolds stress-transport for open-channel flows, Friction Reynolds numbers $Re\tau = 150$, 400, and 1020, J. Hydraul. Res. **59**, 36 (2021).

[36] R. Rasool, N. Chakraborty, and M. Klein, Effect of non-ambient pressure conditions and Lewis number variation on direct numerical simulation of turbulent Bunsen flames at low turbulence intensity, Combust. Flame **231**, 111500 (2021).

[37] A. Gruber, E. S. Richardson, K. Aditya, and J. H. Chen, Direct numerical simulations of premixed and stratified flame propagation in turbulent channel flow, Phys. Rev. Fluids **3**, 110507 (2018).

[38] J. Bailey and E. S. Richardson, DNS analysis of boundary layer flashback in turbulent flow with wall-normal pressure gradient, Proc. Combust. Inst. **38**, 2791 (2021).

[39] U. Ahmed, A. L. Pillai, N. Chakraborty, and R. Kurose, Surface density function evolution and the influence of strain rates during turbulent boundary layer flashback of hydrogen-rich premixed combustion, Phys. Fluids **32**, 055112 (2020).

[40] C. Dopazo, J. Martín, and J. Hierro, Local geometry of isoscalar surfaces, Phys. Rev. E **76**, 056316 (2007).

[41] H. Abe, H. Kawamura, and Y. Matsuo, Direct numerical simulation of a fully developed turbulent channel flow with respect to the Reynolds number dependence, J. Fluids Eng. **123**, 382 (2001).

[42] H. Kolla, E. R. Hawkes, A. R. Kerstein, N. Swaminathan, and J. H. Chen, On velocity and reactive scalar spectra in turbulent premixed flames, J. Fluid Mech. **754**, 456 (2014).

[43] T. Echekki and J. H. Chen, Unsteady strain rate and curvature effects in turbulent premixed methane-air flames, Combust. Flame **106**, 184 (1996).

[44] T. Echekki and J. H. Chen, Analysis of the contribution of curvature to premixed flame propagation, Combust. Flame **118**, 308 (1999).

[45] R. Sankaran, E. R. Hawkes, J. H. Chen, T. Lu, and C. K. Law, Structure of a spatially developing turbulent lean methane-air Bunsen flame, Proc. Combust. Inst. **31**, 1291 (2007).

[46] N. Chakraborty and R. S. Cant, Influence of Lewis number on curvature effects in turbulent premixed flame propagation in the thin reaction zones regime, Phys. Fluids **17**, 105105 (2005).

[47] S. H. Kim and H. Pitsch, Scalar gradient and small-scale structure in turbulent premixed combustion, Phys. Fluids **19**, 115104 (2007).

[48] F. E. Marble and J. E. Broadwell, *The Coherent Flame Model for Turbulent Chemical Reactions*, Technical report, Purdue University, West Lafayette, Indiana, USA, TRW-29314-6001-RU-00. Project SQUID, 1977.

[49] S. Candel and T. J. Poinsot, Flame stretch and the balance equation for the flame area, Combust. Sci. Technol. **70**, 1 (1990).